Ocean Engineering 237 (2021) 109634

Contents lists available at ScienceDirect

Ocean Engineering

journal homepage: www.elsevier.com/locate/oceaneng

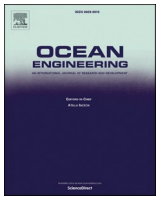

Projecting changes in explosive cyclones and high waves around Japan using a mega-ensemble projection

Junichi Ninomiya [a,*], Yuya Taka [b], Nobuhito Mori [c]

[a] Kanazawa University, Ishikawa, 920-1192, Japan
[b] Pacific Consultants Co., Ltd., Tokyo, 101-8462, Japan
[c] Kyoto University, Kyoto, 611-0011, Japan

ARTICLE INFO

Keywords:
Extratropical cyclone
Explosive cyclone
Climate change
High waves
Large ensemble
d4PDF

ABSTRACT

In this study, we evaluate the effect of climate change on explosive cyclones (ECs) using mega-ensemble projection data (d4PDF), which has 50 members of 60-years present climate experiments and 90 members of 60-years +4K future climate experiments. Subsequently, we evaluate the future change of coastal hazards due to high-swell waves, called Yorimawari waves, caused by strong and stagnant ECs around Japan. The number of ECs passing over the Sea of Japan increased, but the number passing over the Pacific Ocean decreased under future climate. The annual average of the minimum central pressure (MCP) of the EC did not change, but the 10- to 60-year probability value increased for the future. Wave simulations with the d4PDF wind conditions for ECs with an MCP of the 10-year probability value that stagnated for over 24 h around Hokkaido, were conducted. The ensemble average of the maximum significant wave height increased from 0.5 to 1.0 m along the Sea of Japan. The significant wave period increased by over 0.25 s. However, the standard deviation was as large as the wave height of future change. The wave height of high waves depends on the characteristics of the EC.

1. Introduction

The latest IPCC (Intergovernmental Panel on Climate Change) Special Report on the Ocean and Cryosphere in a Changing Climate (SROCC) (IPCC, 2019) indicates that the intensity of extreme phenomena will increase due to climate change. An explosive cyclone (EC), also known as a bomb cyclone, is an extreme phenomenon that occurs around Japan in winter, especially in the northern part of Japan. It is defined as an intensive extratropical cyclone, which decreases by approximately 24 hPa or more at the center of the cyclone in 24 h (Sanders and Davis, 1988). Its characteristics, such as, an asymmetric structure, its occurrence between October and March, and stagnating for a long period of over 24 h, differ from those of typhoons. Japan has suffered from coastal disasters due to ECs. For example, on February 24, 2008, large swells with a significant wave height of 9.92 m and a significant wave period of 16.2 s at the Toyama point (20 m depth) by Japanese wave observation network, NOWPHAS (Nationwide Ocean Wave information network for Ports and HArbourS), were induced by an EC in Japan. This swell event caused 1 casualty and 15 injuries along coastal area of Toyama Bay in the Sea of Japan (Kawasaki et al., 2008; Ranasinghe et al., 2010). On December 16, 2014, an EC induced an approximately 1.7 m storm surge that caused inundation at Nemuro in Hokkaido (Saruwatari et al., 2014; Bricker et al., 2015). The EC disasters are not unique to Japan; they are also found in North America and Europe (Feser et al., 2015; Bärring and von Storch, 2004; Gulev et al., 2001). Some studies have indicated that the observed frequency and intensity of ECs in winter over the last few decades has increased, and this trend is projected to continue in the future (Graham and Diaz, 2001; Langenberg et al., 1999).

Several studies related to ECs in Japan have been conducted. Mori et al. (2017) analyzed the characteristics of ECs around Japan in the past 55 years using the Japanese 55-year reanalysis (JRA-55) by the Japanese Meteorological Agency. They demonstrated that although the genesis frequency of the EC exhibited a decreasing trend weakly, the intensity of them, especially strong EC, showed an increasing trend since 1958. Yoshida and Asuma (2004) summarized the characteristics and development mechanism of ECs based on three classified tracks, as well as their development related to the eddies at upper and lower air, the latent heat flux from the sea surface in the Pacific Northwest.

To investigate the effect of climate change on coastal disasters in East Asia, Shimura et al. (2014) estimated future changes in wave climates based on horizontal 60 km resolution wave projections using the

* Corresponding author. Kanazawa University Kakuma, Kanazawa, 920-1192, Japan.
E-mail addresses: jnino@se.kanazawa-u.ac.jp (J. Ninomiya), yuuya.taka@tk.pacific.co.jp (Y. Taka), mori@oceanwave.jp (N. Mori).

https://doi.org/10.1016/j.oceaneng.2021.109634
Received 27 January 2021; Received in revised form 15 June 2021; Accepted 6 August 2021
Available online 13 August 2021

Meteorological Research Institute Atmospheric General Circulation model (MRI-AGCM3.2H) and showed an increasing trend of the maximum wave heights in eastern Japan due to climate change. However, research on future changes in regional coastal disasters has been performed based on a small number of ensemble results using time-slice experiments (typically 20–25 years); however, statistical evaluations of low-frequency phenomena are difficult to perform based on a small number or decal length of experiments. Therefore, Mori et al. (2016) conducted mega-ensemble projections using the database for policy decision making for future climate change (d4PDF), integrating over 5000 years of both present and future +4K warmer climate conditions. Mori et al. (2016) evaluated future changes in storm surges caused by typhoons using d4PDF, which is a large climate dataset comprising data of extreme events over 100 years, and showed an increase in storm surge height of approximately 0.5 m for the 100-year probability value in Osaka Bay, Japan. However, studies regarding future changes in ECs and coastal disasters caused by climate change are rare.

In this study, we evaluate the effect of climate change on ECs involving in disasters in Japan using d4PDF and investigate the future change of coastal hazards due to ECs, in particular *Yorimawari* waves in the Sea of Japan. First, outline of EC dataset based on d4PDF is explained in detail. Second, the changes in EC characteristics due to climate change is analyzed targeting around Japan. Third, the application of EC dataset to *Yorimawari* waves is investigated in the northern part of Japan.

2. Methodology

2.1. Overview of dataset

2.1.1. d4PDF climate projection dataset

A future scenario was developed using the mega-ensemble projection for climate change, d4PDF, by performing a large number of climate simulations using high-resolution global and regional atmospheric models (Mizuta et al., 2017). Simulation experiments were designed such that past climate signals and future changes in mean climate and extreme events, such as heavy rainfall and tropical cyclones, can be detected with high statistical confidence. In d4PDF simulations, global surface air temperatures are climatologically constant at +4 K, relative to post-industrial levels, corresponding to the end of the 21st century in the RCP8.5 (Representative Concentration Pathway) scenario experiments of the CMIP5 (Coupled Model Intercomparison Project 5) participating models. Global/General and regional circulation/climate models (GCM and RCM) of 60 and 20 km meshes were used for present and future climate simulations, respectively. The 60 km mesh resolution was approximately twice as high as those of most CMIP6-participating models in order to decrease calculation cost and increase the number of ensemble members. Reproduce of Extreme events, such as typhoons, needs several kilometers resolution, so GCM may weakly estimate extreme events. GCM used in the simulation was the Meteorological Research Institute atmospheric general circulation model version 3.2 (MRI-AGCM3.2) (Mizuta et al., 2012), and the regional model was MRI nonhydrostatic regional climate model (NHRCM) (Sasaki et al., 2011; Murata et al., 2013) covering the Japan Islands to investigate various effects of climate change on Japan (Fig. 1). The ensemble members of every experiment exceeded 50, and a pair of both global and regional simulations was available for each simulation type.

All simulations were conducted by integrating the models forced by the prescribed sea surface temperature (SST) and sea ice concentration (SIC). Future SSTs and SICs used in these simulations were detrended observations added to the SST future change distribution of CMIP5 RCP8.5 experiments using six different atmosphere-ocean GCMs. The uncertainties in the CMIP5 scenario experiments were accounted for by the future change of the six CMIP5 models. Selected six CMIP5 models were CCSM4 (CC), GFDL CM3 (GF), HadGEM2-AO (HA), MIROC5 (MI), MPI-ESM-MR (MP) and MRI-CGCM3 (MR). The results of d4PDF have been widely analyzed and applied to different sectors of impact assessment in Japan (Ishii and Mori, 2020).

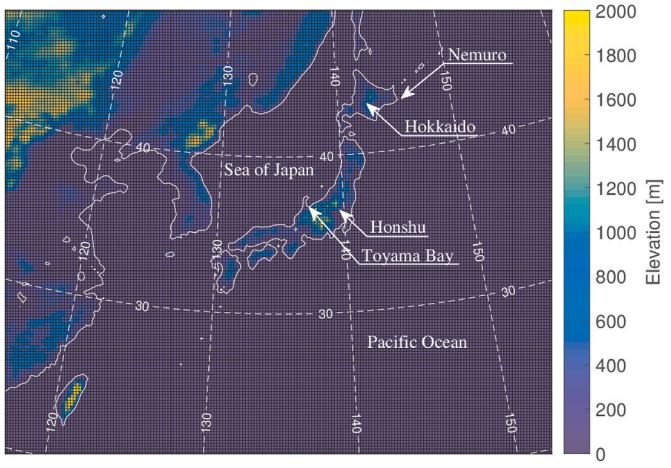

Fig. 1. Domain of regional model of d4PDF.

We analyzed the EC using the d4PDF RCM experiment results. The d4PDF had a 20-km horizontal and 1-h temporal resolution. The d4PDF was performed under observed SST with 50 kinds of perturbations in present climate and under six future SSTs with 15 kinds of perturbation in future climate experiment as the initial and boundary conditions.

(1) Present Climate Experiment: September 1950–August 2011 (60 years) × 50 Members, Total: 3000 years
(2) +4K Future Climate Experiment: September 2050–August 2111 (60 years) × 90 Members (6 GCMs × 15 perturbation), Total: 5400 years

The conditions of +4K future climate experiments were defined as the constant conditions in which the global average temperature increased by 4K compared with the age of the Industrial Revolution (1850). Because the global warming trend was not included throughout the experimental period, the comparison between +4K future climate experiments and non-warming experiments is able to evaluate the impact of climate change. Since there are not non-warming experiments of d4PDF RCM, a rigorous comparison with pre-industrial climate is not possible. However, the similar line in previous study analyzing JRA-55 by Mori et al. (2017) showed only a weak trend that cannot be distinguished from natural variability in both intensity and frequency from 1958 to 2011. Based on their finding this study compares the present climate experiments with +4K future climate. The variables of d4PDF dataset used in this study are SLP (sea level pressure) and U10/V10 (eastward/northward wind at 10 m height).

2.1.2. JRA-55 reanalysis atmospheric dataset

The Japanese 55-year Reanalysis (JRA-55) is one of the latest reanalysis dataset of atmosphere (Kobayashi et al., 2015). JRA-55 provides data on atmospheric variables at 60 km horizontal grids. Its resolution is coarse to reproduce the extreme atmospheric phenomena, but JRA-55 has high reliability around Japan and the other regions due to the data assimilation. JRA-55 is used to evaluate the present climate experiment of d4PDF. JRA-55 faithfully reproduces historical environment. However, historical environment does not represent climatic values. We must be careful that the variables based on large number of samples, such as monthly averaged temperature and daily precipitation, in JRA-55 will be included in the probability distribution of d4PDF, while the variables based on small number of samples in JRA-55 may be outlier of d4PDF.

2.2. Method of extracting EC

We developed a standard and fast extracting EC method for long-term d4PDF. Developed method uses spatial and temporal changes in SLP for the analysis period from October to April. The EC is defined as an extratropical low-pressure which the central pressure drops more than $24[\mathrm{hPa}] \times \sin\phi/\sin 60^\circ$ (ϕ is the latitude [degree]) in 24 h by Japan Meteorological Agency. Fig. 2 illustrates the algorithm for detecting and tracking the EC. The extraction procedure comprised following three steps.

Step 1. pertains to the search for the cyclone center. First, the SLP spatial distribution was smoothed by a Gaussian filter to remove the noise that caused the error. We removed the grids at altitudes higher than 1500 m because the grids had a lower SLP because of the error from sea level correction. Subsequently, the grid that was at least 1 hPa smaller than the average SLP surrounding grids was extracted as a candidate for the center of the cyclone for every snapshot. When multiple centers were detected in a 3° radius area, the center with the smallest SLP was selected.

Step 2. involves tracking the extracted cyclone center in Step 1. The detection area of the next time-step center was within travel distances of 1.5°/h to the east and west and 1.0°/h to the north and south, respectively. If multiple centers are detected in the detection area, then the center with the smallest SLP is selected as the next time-step center. We set the lifetime of the cyclone to be more than 24 h in order to exclude the disappeared low-pressure due to the fusion of multiple low-pressures.

Step 3. is to assess whether the tracked cyclone in Step 2 is an EC. We set two criteria: occurrence season and the maximum development rate of the central pressure. The EC typically occurred during winter and spring in the target region, i.e., from November to April. Yoshida and Asuma (2004) defined the development rate as

$$\varepsilon = \frac{p(t-12) - p(t+12)}{24} \times \frac{\sin 60^\circ}{\sin\phi(t)}$$

where p is the central pressure of the cyclone in SLP [hPa], t is the time [h], and ϕ is the latitude [degree]. The development rates for d4PDF and JRA-55 are calculated every 1 hour and every 6 hours, respectively. Subsequently, the maximum development rate of the central pressure of 1.0 or more is judged as EC.

The influence of temporal resolution to the calculation of development rate is small. Although this extracting algorithm does not distinguish a typhoon from an EC, for the atmospheric reanalysis dataset (JRA-55), it extracted 1047 ECs, including two typhoons (0.19%) over 60 years. This algorithm is simple, fast, and sufficiently accurate. In the following section, we analyze the calculated EC database.

2.3. Wave modeling

We evaluate the Yorimawari wave that is one of the high wave events in winter at Toyama Bay in Japan. Generally, Yorimawari wave is defined by their generation process, and there are various criteria for the observed wave height and period. For example, the significant wave height and period are more than 1 m and 10 s, or more than 2 m and 8 s. Yorimawari wave is caused by strong and stagnant ECs around east coast of Hokkaido and seasonal pressure distribution in winter. The strong pressure gradient causes strong northerly winds over the eastern Sea of Japan, which develops high waves. Developed high waves reach Toyama Bay, which has a steep and complex topography, and bring disaster to the Toyama coastal area (Tamura et al., 2020).

The future change of extreme waves caused by the extreme ECs is investigated by the spectral wave modeling. Simulating Waves Nearshore, Ver. 41.10 (SWAN) (Booij et al., 1999) is used. SWAN is one of the open-source models and is used in many researches. In this study, SWAN is forced by the wind fields (U10 and V10) of d4PDF RCM (20 km resolution) for ECs. The calculation domain used in SWAN is 135–150° east longitude and 36–46.5° north latitude with 0.1° resolution. The directional resolution is 10°, and the frequency is set from 0.05 to 1.0 Hz with 30 bins. The calculation period is the duration when the ECs were extracted. Bathymetry is interpolated from GEBCO 2014. Calculation conditions are activated with default parameters of SWAN. Tamura et al. (2020) showed that it is difficult to reproduce the waves along the coast of Toyama Bay with a spectral wave model. We extract the ECs that cause Yorimawari wave and evaluate the swells at the mouth of Toyama Bay.

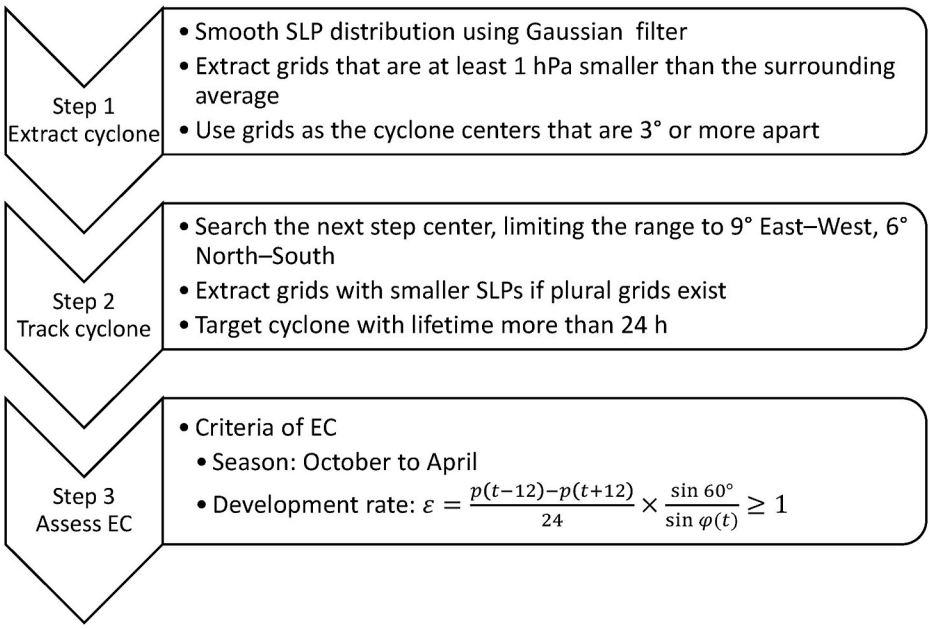

Fig. 2. Algorithm of detecting and tracking EC.

3. Analysis results and discussion

3.1. Frequency of ECs

To investigate the future change in the number of ECs around Japan due to climate change, we compared the characteristics of the extracted EC under the present and future climates of the d4PDF. Furthermore, we compared the reanalysis data JRA-55 to validate the present climate simulation of d4PDF. In Table 1, the annual average numbers of extracted ECs in JRA-55 and d4PDF in the present and future climates, respectively, are shown. The results of the future climate show each SST ensemble. The baseline EC frequency by JRA-55 was 17.45/y. The frequency of d4PDF in the present climate was 10.15/y based on the 50-case ensemble average, whereas that in the future climate was 10.56/y based on the 90-case ensemble average. The EC frequency by JRA-55 indicates a larger number of occurrences than that by the d4PDF in the present climate owing to the differences in modeling conditions between JRA-55 and d4PDF due to the general circulation model and RCM, data assimilation, and horizontal resolution. However, it is difficult to discuss the differences in the model characteristics from this result. Regarding data assimilation and horizontal resolution, some studies reported that high-resolution modeling and using data assimilation reproduced accurate typhoons, but the literature on ECs is limited. Although JRA-55 is a 60 km global reanalysis with a lower resolution than the regional d4PDF dataset (20 km), data assimilation is effective for reproducing the EC. The differences between JRA-55 and d4PDF present climate runs require further studies.

The d4PDF in the future climate estimates a slightly larger number than that in the present climate. The standard deviations in the present and future climates were 2.09 and 0.71, respectively. The *t*-test for the number of ECs around Japan showed that the future change in the number of EC was not statistically significant at the $p = 0.05$ level, and an increasing trend was not significantly detected. Furthermore, the results for each SST change pattern presented a small standard deviation from 0.27 to 0.41. The distribution of SST may be related to the number of occurrences of ECs; however, we did not obtain a characteristic parameter between the SST change distribution around Japan and the number of ECs. A more detailed analysis including daily changes in SST and cyclone development is necessary.

3.2. EC track

In Fig. 3, the annual average frequencies of EC track in JRA-55, present and future climate conditions of d4PDF are shown. The EC tracks can be classified into two major routes. One is over the Sea of Japan and the other is along the southern coast of Japan over the Pacific Ocean. These tracks in JRA-55 and d4PDF agree with the previous results of Yoshida and Asuma (2004). Although the frequency distributions of ECs in JRA-55 and d4PDF in the present climate are similar, the estimated number of ECs in d4PDF is underestimated by approximately 62% over the Pacific Ocean and 30% over the Sea of Japan compared to JRA-55.

The frequency of ECs along the Pacific side in d4PDF in the present climate was three times larger than that on the Sea of Japan side. The average frequency of ECs passing along the southern coastal area of Honshu Island was 1.1/y in present climates. Meanwhile, the future change in the intensity of ECs over the Sea of Japan was stronger than

Table 1
Ensemble-averaged value and standard deviation of annual number of explosive cyclones. CC, GF, HA, MI, MP, and MR indicate different ensembles of d4PDF future climate runs. (CC: CCSM4, GF: GFDL-CM3, HA: HadGEM2-AO, MI: MIROC5, MP: MPI-ESM-MR, MR: MRI-CGCM3).

		Average	S.D.
JRA-55		17.45	
Present (n = 50)		10.15	2.09
+4K Future (n = 90)		10.56	0.71
SST pattern in future (each n = 15)	CC	10.01	0.33
	GF	10.23	0.33
	HA	9.67	0.27
	MI	11.39	0.27
	MP	11.17	0.34
	MR	10.91	0.41

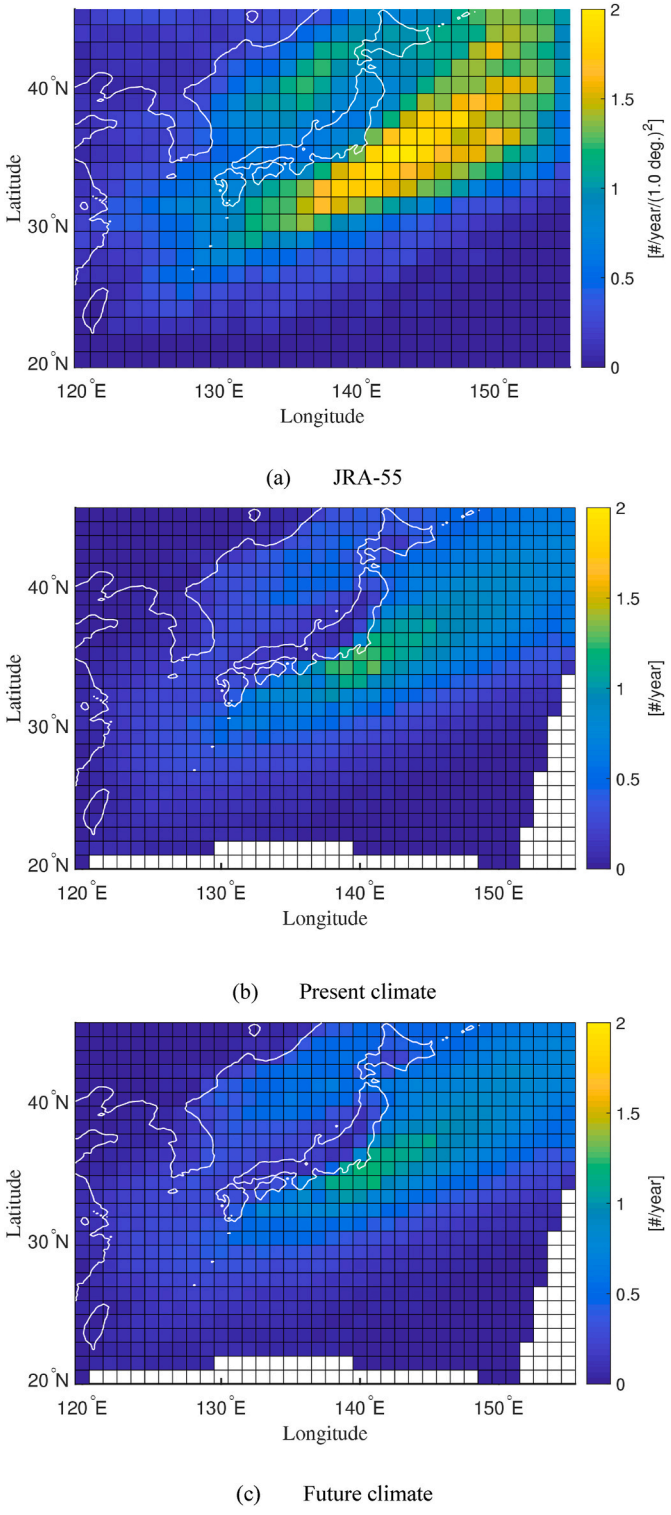

Fig. 3. Annual average frequency of passing explosive cyclones in JRA-55 and d4PDF (The result of JRA-55 is plotted every 1.25° but scaled to 1°. The results of d4PDF are plotted every 1°. units: #/year).

that on the Pacific side. The details of the intensity change of ECs will be discussed in the next section.

Fig. 4 shows the future changes in the frequency of ECs (future minus present). Fig. 4 (a) shows that the mean frequency change of ECs over the Pacific Ocean decreased in the future climate, whereas the frequency passing over the Sea of Japan increased by the same magnitude. In addition, the trends of future changes in frequency over the Pacific Ocean and the Sea of Japan were rejected at 95% by the *t*-test and shown to be statistically significant. The main cause of the frequency changes was the northward shift of the westerly winds due to climate change, which is consistent with IPCC SROCC (IPCC, 2019) and other recent studies. The magnitudes of the frequency changes were −10% over the Pacific Ocean and +28% over the Sea of Japan compared with the frequency in the present climate (Table 2). The future change in the frequency under each SST pattern is shown in Fig. 4 (b). Almost all trends of future change agreed with the ensemble average, but the frequency under the MI condition increased over the Pacific Ocean. The d4PDF in the future climate estimated a shift in the EC track from south to north, and a part of the SST pattern suggested that it would affect the EC track.

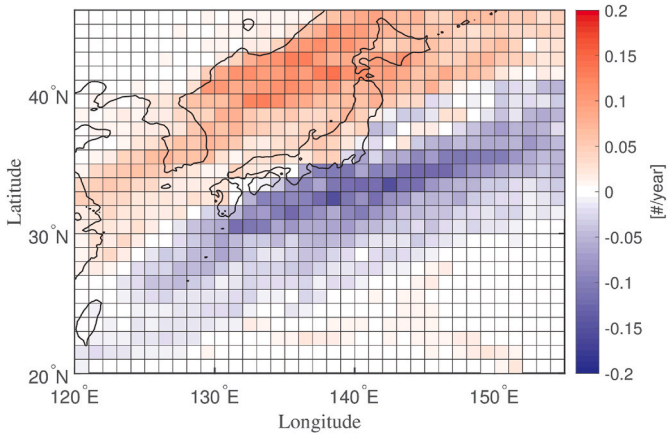

(a) Entire ensemble average

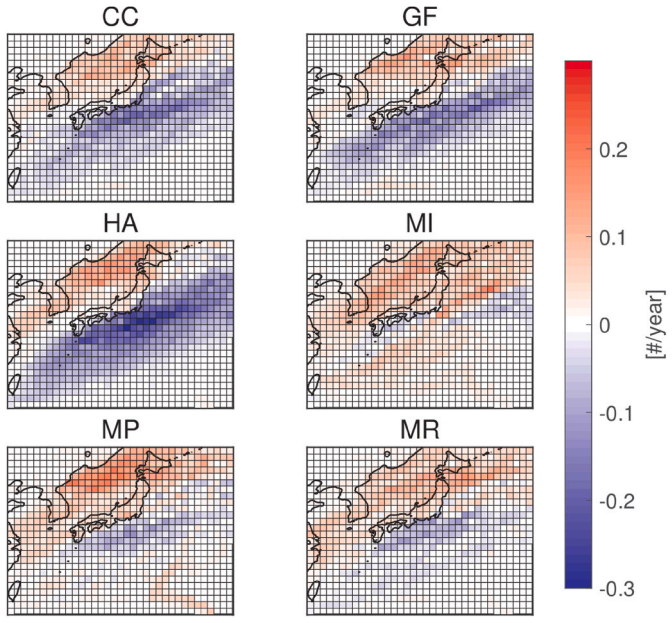

(b) Each +4K SST pattern

Fig. 4. Future change in passing frequency of explosive cyclones (units: #/year).

Table 2
Annual mean number of explosive cyclones by track (units: #/year).

		Over the Sea of Japan (Passing the meridian of 138°E above 37°N)	Over Pacific Ocean (Passing the meridian of 138°E below 35°N)
JRA-55		7.02	6.61
Present		2.41	3.30
+4K Future		3.09	2.98
SST pattern in future	CC	2.94	2.78
	GF	2.95	2.80
	HA	3.30	2.64
	MI	2.97	3.28
	MP	3.28	3.19
	MR	3.11	3.20

As spatial patterns of SST were forced in the MRI-AGCM, all patterns can occur in the same RCP scenario. The changes in the SST patterns at the global scale indicated significant differences in the regional-scale climate.

3.3. Central pressure of extreme ECs

As the average frequency of ECs will be increased, as shown in Table 2, it is important to analyze future changes in ECs. Table 3 shows the annual mean minimum central pressure of ECs by track. The ECs in the present climate are stronger than those of the JRA-55, and the averaged intensity of ECs is not consistent with JRA-55. Future change indicates enhancements. Fig. 5 (a) shows the return period of the minimum central pressure (MCP) of the EC based on extreme value analysis in the present and future climate conditions. The return periods are calculated from the ranking of MCPs in each 60-year ensemble member. The hatched areas are the envelopes of maximum and minimum values by the ensemble members in the present and future climate. The thick lines indicate the ensemble-averaged values. The black line represents the extreme distribution by JRA-55. The extreme EC intensity by JRA-55 estimated a stronger EC below the 10-year return period than the strongest member of the d4PDF in the present climate; however, the intensity of the EC from a 10- to 60-year return period in JRA-55 included the range of d4PDF members. It should be noted here that the past reanalysis only represents one scenario in the past climate. Although the weak ECs of d4PDF in the present climate were underestimated based on the JRA-55, d4PDF yielded a reasonable estimation of strong ECs. The variance of each ensemble member was 17 hPa in the present climate and 29 hPa in the future climate at a 60-year return period, and the difference in the ensemble averages of the present and future climates was approximately 2–3 hPa from the 1- to 60-year return period. The averages of all ECs' MCP around Japan in the present and future climates were 980.6 and 980.2 hPa, respectively. The longer return period estimated a larger future change in the MCP of the EC. Extreme ECs below 970 hPa will increase in future climate conditions (Fig. 6). Fig. 5 (b) shows the ensemble-averaged MCP for fixed SST

Table 3
Annual mean minimum central pressure of explosive cyclones by track. (SST patterns in future means the SST distribution patterns of future change in d4PDF experiments.)

		Over the Sea of Japan	Over Pacific Ocean
JRA-55		978.1	980.7
Present		953.2	948.3
+4K Future		949.6	946.6
SST pattern in future	CC	949.0	944.8
	GF	949.5	944.1
	HA	950.9	948.0
	MI	951.7	946.9
	MP	949.2	949.7
	MR	947.2	945.6

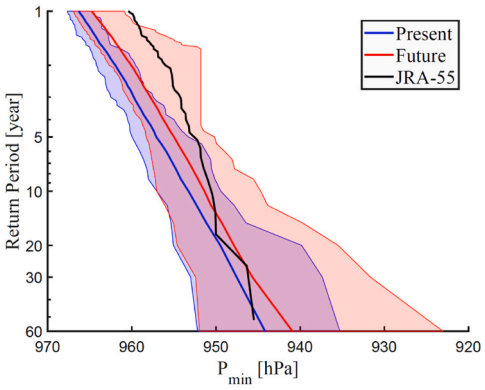

(a) Comparison among JRA-55 (black), d4PDF in the present (blue), and future climate (red). The thick lines indicate the ensemble average, and the hatched areas indicate the envelopes of the maximum and minimum values by the ensemble members.

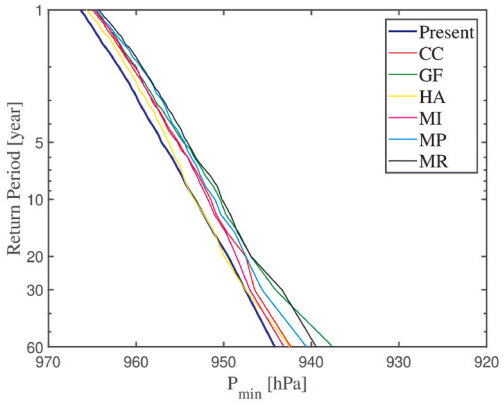

(b) Comparison among d4PDF in the present and future SST patterns.

Fig. 5. Return period of minimum central pressure of explosive cyclones around Japan.

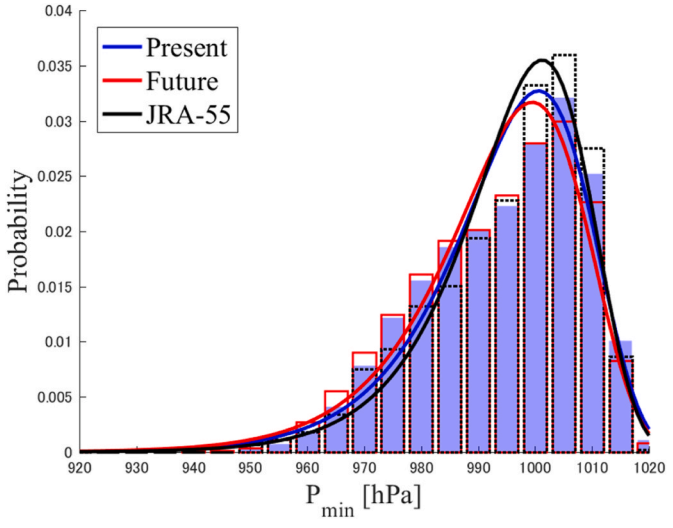

Fig. 6. Probability distribution of minimum central pressure of explosive cyclones around Japan (blue bars: d4PDF present climate, red bars: d4PDF +4K climate, black bars: JRA-55, solid lines indicate fitted distributions with a Weibull function). (For interpretation of the references to color in this figure legend, the reader is referred to the Web version of this article.)

patterns and the present climate condition. The distributions of CC, HA, MI, and MP indicated almost the same profiles as that of the 60-year return period, which was 2–3 hPa stronger than that of the present climate. The distributions of GF and MR indicated a decrease of approximately 7 and 5 hPa in the 60-year return period, respectively. Provided that the strong ECs have a longer return period, the intensity of the MCP will increase in any of the SST patterns. Similarly, the intensity of ECs varies depending on the SST pattern as well as the occurrence and passing frequency of ECs; however, the variability of intensity due to SSTs is larger than the average future change signal.

3.4. Local EC characteristics

Extreme ECs caused severe coastal disasters in the northeastern part of Japan in the winter. Next, we analyze the characteristics of ECs in the present and future climate conditions, classified into smaller domains in Northeast Japan. The translation speed and central pressure of ECs were analyzed for 11 domains, as shown in Fig. 7. We compared the results of reanalysis data JRA-55 and d4PDF, verified the agreement between JRA-55 and the d4PDF in the present climate, and evaluated the future change in the d4PDF.

Fig. 8 shows the box-and-whisker plot of the annual average of translation speed of the EC for each domain. The left and right plots of each domain indicate the results in the present and future climates, respectively. The circles in the present climate indicate the annual average value of JRA-55. The upper and lower lines of the box indicate the first and third quartiles, respectively, and the horizontal line in the box is the median value. The upper and lower whiskers are the maximum and minimum values within the quartiles range plus 1.5 times the quartiles, respectively. The translation speed of ECs in JRA-55 by the domains is within the range of the whiskers of the d4PDF in the present climate. The translation speed decreased as the latitude increased. The d4PDF estimated the increasing translation speed in Northeast Japan in the future. The future change signal became significant to the north, which is related to future changes in large-scale circulations.

Fig. 9 shows future changes in zonal wind speed at 500 hPa from October to April. The zonal wind speed will increase above 40N, which corresponds to domains 2, 4, 5, 7, 8, 10, and 11 in Fig. 7. The increase in the translation speed of the EC is consistent with the zonal wind distribution shown in Fig. 9. On the other hand, the future changes in zonal wind speed in domains 1 and 3 will decrease and affect the southern domains below 40N.

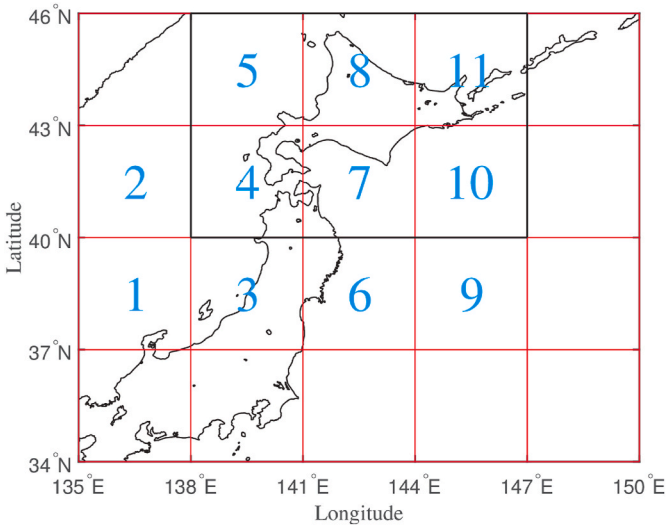

Fig. 7. Analysis domain of an explosive cyclone (Blue colored number: domain number). (For interpretation of the references to color in this figure legend, the reader is referred to the Web version of this article.)

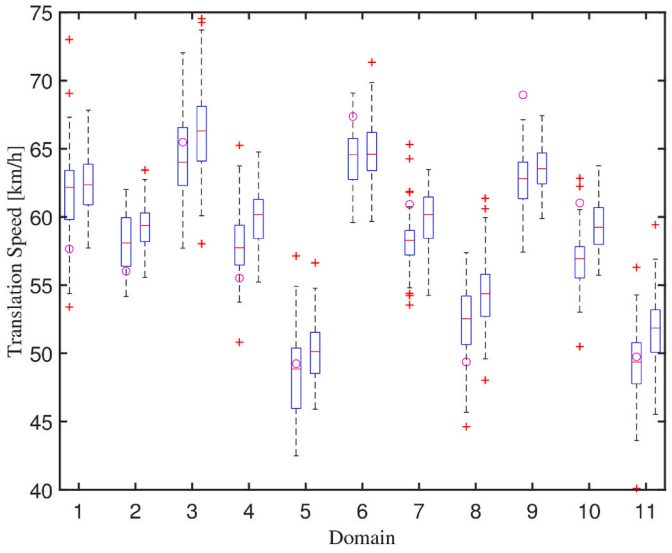

Fig. 8. Box-and-whisker plot of annual average translation speed of explosive cyclones in each domain shown in Fig. 7. (Left: present climate of d4PDF, right: future climate of d4PDF, circle: mean of JRA-55, box: first and third quartiles, line in box: median value, upper (lower) of broken line: maximum (minimum) value within 2.5 times of quartile range, plus: outlier).

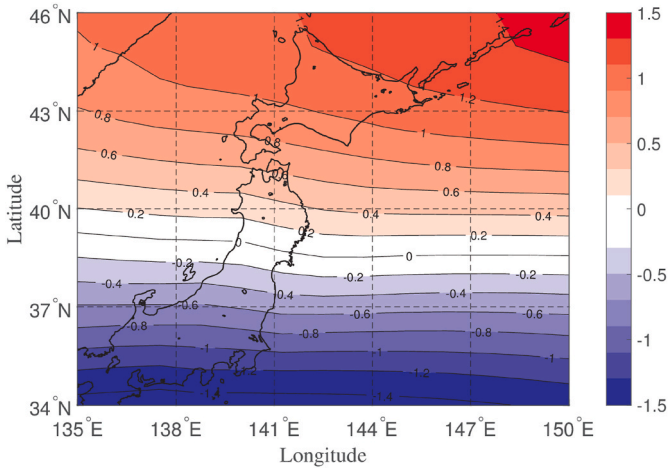

Fig. 9. Future change of zonal wind at 500 hPa from October to April (Red shading: increasing westerly wind speed; blue shading: decreasing westerly wind speed). (For interpretation of the references to color in this figure legend, the reader is referred to the Web version of this article.)

A similar analysis was performed for the intensity of ECs. Fig. 10 shows the box-and-whisker plot for the MCP of ECs by domain. Fig. 10 (a) and (b) show the annual average value and the 10-year probability value. JRA-55 in almost of all domains is within the range of whiskers of both the annual average value and 10-year probability value in the present climate. Annual average value of JRA-55 in the domains 1, 5 and 8 are out of the range of d4PDF in present climate. Since the number of weak ECs in JRA-55 is more than those in d4PDF (Table 1 and Fig. 6), the average intensity of EC in JRA-55 is weaker than that in d4PDF. This feature depends on the domain, and the domains 1, 5 and 8 show clearly.

The MCP decreased as the longitude and latitude increased in both climates. The MCP decreased from the west to east due to the development route of the system, although the range of annual average value of MCP between the present and future climate conditions differed slightly. Meanwhile, the 10-year return values in the future climate of all domains were estimated to be smaller than those in the present climate.

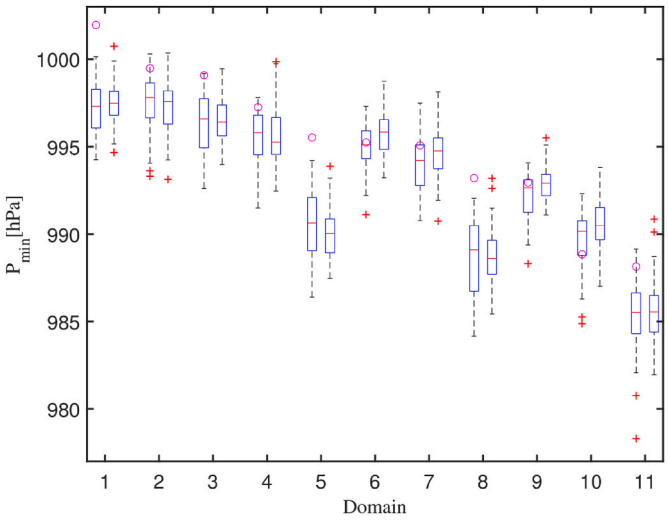

(a) Annual average value

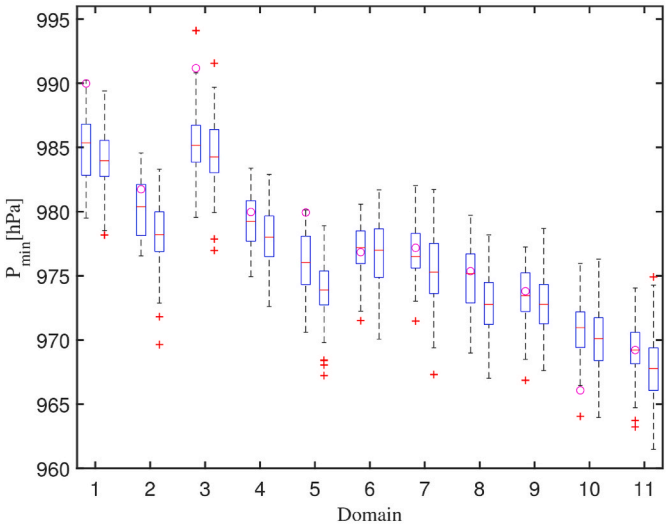

(b) 10-year probability value

Fig. 10. Box-and-whisker plot of 1- and 10-year probability minimum central pressure of explosive cyclones in each domain (The meanings of each plot are the same as those in Fig. 8).

The differences were remarkable in the high-latitude domain. The average future changes in the annual average value and the 10-year return value of all domains were +0.3 and −1.2 hPa, respectively. Their first quartiles were +0.5 and −1.9 hPa, respectively, and their lower whisker values were +1.1 and −2.2 hPa, respectively. These results show that the annual average amplitude of the EC did not change or will be weaker, and the ECs with a 10-year probability amplitude will be stronger. In summary, the EC are projected to become extreme, and the scale of coastal disasters will increase, e.g., the high waves in Toyama Bay in 2008 (Lee et al., 2010) and storm surges in Nemuro in 2014 (Saruwatari et al., 2015).

4. Future changes in extreme waves by ECs

One of the coastal disasters due to ECs is high waves along the Sea of Japan, which is called *Yorimawari* waves locally. The development

factor of high waves in the winter is strong north winds off the western coast of Hokkaido and the northwest coast of the Honshu area due to the strong EC propagating extremely slowly or stagnating around Hokkaido. Analyses of ECs and related high waves around Hokkaido are important to reduce wave-related disasters in the northern part of Japan. The target area for analysis is the same as that in Section 3.4. We simulated high waves due to strong and stagnant ECs under both climate conditions. As the number of ensembles of d4PDF was large for computation, the calculation period was limited by the strength and stagnation of ECs. The conditions of the ECs to be used for calculation were that ECs have stronger MCP than the 10-year return value in the present and future climate conditions in domain 2 and that ECs stagnated around Hokkaido (corresponding to the domains 4, 5, 7, 8, 10 and 11 in Fig. 7) for more than 24 h. The extracted ECs were 17 cases in the present climate and 22 cases in the future climate, which were unevenly due to a northward track shift in the present and future climate conditions. Fig. 11 shows the selected EC tracks and the bold lines mean averaged tracks in the present and future climate. Although the averaged tracks differed by 1.5–2.0°, it would not have a significant impact on the estimation of high waves because the spatial scale of the bomb cyclone was 1000 km.

The extreme wave climate for the selected extreme ECs was simulated using the spectral wave model forced by the wind field of d4PDF RCM for all extracted ECs. Fig. 12 shows the spatial distribution of the ensemble-averaged maximum significant wave height (MSWH). Fig. 12 (a) and (b) show the average value and standard deviation, respectively. The spatial distribution of the MSWH ranged from 5 to 7 m along the Sea of Japan from the north of Honshu to the Noto peninsula. The distribution of the standard deviation indicated small variations (<1 m) in the area corresponding to a large wave height along the Sea of Japan. The area of larger MSWH with a smaller standard deviation implied that the dependence of high waves on the track of EC was reduced by the criteria of selected events. Meanwhile, the standard deviation in the Pacific Ocean side was large (>1 m). Therefore, the evaluation of high waves in the Pacific Ocean due to the EC required different criteria to select the events. For example, the risk evaluation of Uchiura Bay was performed in the southwest of Hokkaido on the Pacific Ocean side.

Fig. 12 shows the future change in the ensemble-averaged MSWH. The future change of extreme wave height indicated +0.5–1.0 m along the Sea of Japan. The wave height increased beyond 0.75 m off the west coast of Honshu. The future decrease was evident in the east coast of Hokkaido; however, it increased in the offshore region. In addition, the wave height increased beyond 0.5 m at the Ishikari Bay located in

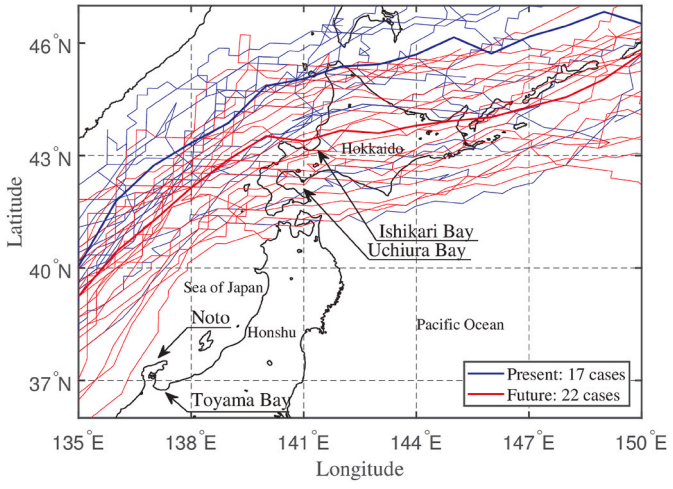

Fig. 11. Tracks of an extracted explosive cyclone have a lower limit of the 10-year probability value of central pressure and stagnate around Hokkaido for more than 24 h (blue: present climate (n = 17); red: future climate (n = 22)). (For interpretation of the references to color in this figure legend, the reader is referred to the Web version of this article.)

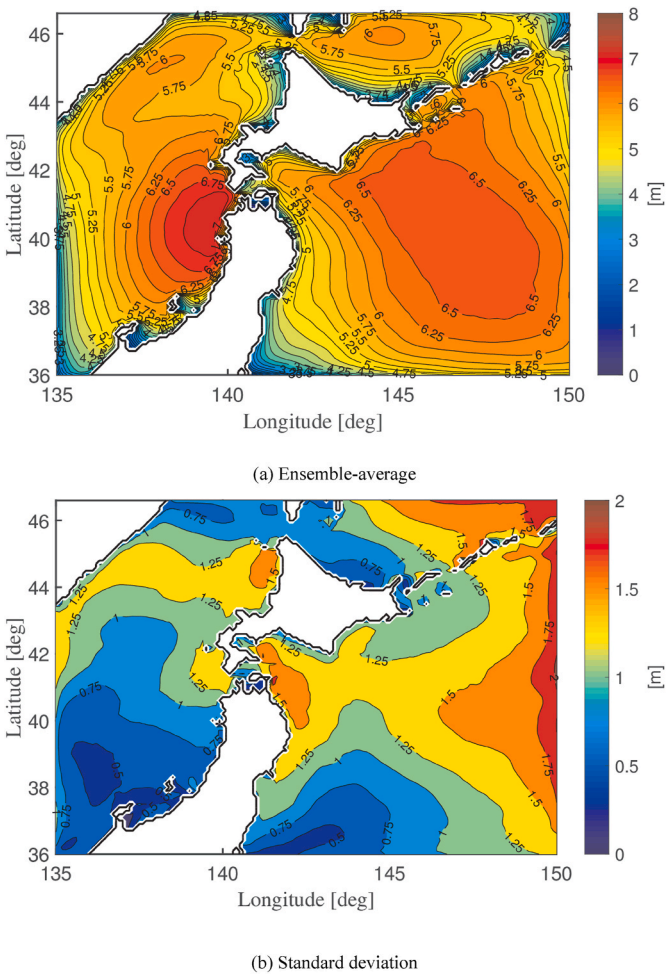

Fig. 12. Distribution of ensemble-average and standard deviation of maximum significant wave height calculated from 17 events under present climate of d4PDF (contour line plots every 0.25 m).

northwestern Hokkaido. The spatial distributions of the MSWH and its changes differed, and future changes in the MSWH differed from those in the zonal wind speed, as shown in Fig. 9. Compared with winds, high waves must develop and propagate long distances. Therefore, the effects of fetch contributed significantly to changes in the MSWH, as shown in

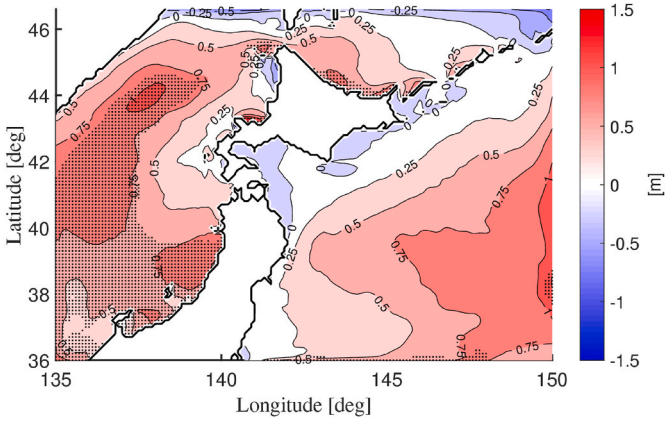

Fig. 13. Future changes in ensemble-average of maximum significant wave height calculated from 22 events under future climate of d4PDF (contour line plots every 0.25 m, and black dotted area means that the future change is statistically significant.).

Fig. 13.

The wave period is also important parameter to evaluate the coastal hazard risk because Tamura et al. (2020) showed that the wave ray trajectories with longer wave period were concentrated in specific locations along the coastal area with the complex topography, such as Toyama Bay. In Fig. 14, the distribution of the significant wave period at the MSWH is depicted. In Fig. 14(a), the ensemble-averaged value of the significant wave period in the present climate is shown, and in Fig. 14 (b), the future change in the ensemble average is depicted. The ensemble average of the significant wave period in the present climate was beyond 10 s along the Sea of Japan. The wave condition along the Sea of Japan was an outstanding swell, and the results of wave height and wave period agreed with the extracting condition for the EC. An increasing distribution was shown in the significant wave period beyond 0.25 s along the Sea of Japan. In particular, for the coastal area from the Toyama Bay to Niigata, a large future change exceeding 0.5 s was estimated. In addition, a similar increasing trend was observed in Ishikari Bay. Based on these results, the strengthening of ECs and the risk of coastal disasters will increase in areas where disasters have occurred in recent years, in terms of both wave height and wave period.

5. Conclusion

We developed a fast and simple algorithm for extracting ECs from SLP. A new algorithm was applied to the large ensemble dataset d4PDF, and the future change analysis of ECs was conducted. Subsequently, we evaluated the risk of high waves caused by ECs. The results obtained in this study are as follows:

- EC tracks were classified into the tracks of the Sea of Japan and Pacific Ocean. The number of ECs that passed over the Pacific Ocean decreased, whereas the number that passed over the Sea of Japan increased significantly.
- The annual average of the MCP of the EC around Japan did not change, but the 10- to 60-year probability value will increase in the future. A detailed analysis based on a small domain showed the same trend regarding the intensity of the EC.
- We conducted wave simulations using the d4PDF wind in the present and future climates. The simulations targeting the Yorimawari wave were conducted for the period when strong ECs were stagnant around Hokkaido. The ensemble-averaged value of the estimated significant wave height increased from +0.5 to +1.0 m along the Sea of Japan. The standard deviation of the significant wave height was small, and we confirmed that the extracting condition targeting the Yorimawari wave yielded good results. The significant wave period at the MSWH along the Sea of Japan increased to beyond 0.25 s.

The method used in this study can be applied to North America and Europe.

Funding

This work was supported by the Integrated Research Program for Advancing Climate Models (TOUGOU) Grant Number JPMXD0717935498 from the Ministry of Education, Culture, Sports, Science and Technology (MEXT), Japan, and by JSPS KAKENHI.

CRediT authorship contribution statement

Junichi Ninomiya: Conceptualization, Methodology, Validation, Resources, Writing – original draft, Writing – review & editing, Visualization, Project administration, Funding acquisition. **Yuya Taka:** Software, Formal analysis, Data curation, Investigation, Visualization. **Nobuhito Mori:** Software, Resources, Supervision, Funding acquisition.

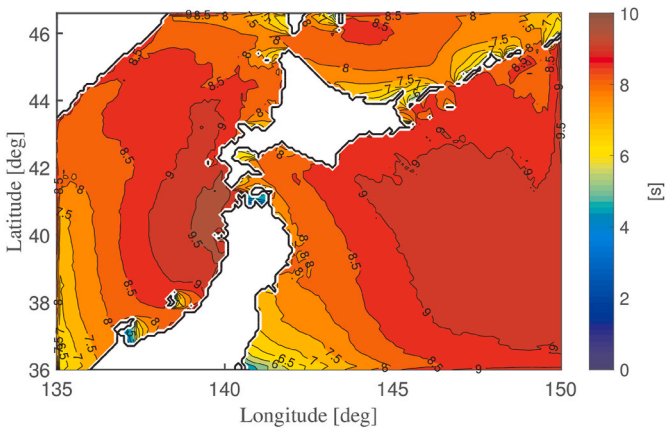

(a) Ensemble average in the present climate (contour line plots every 0.5 s).

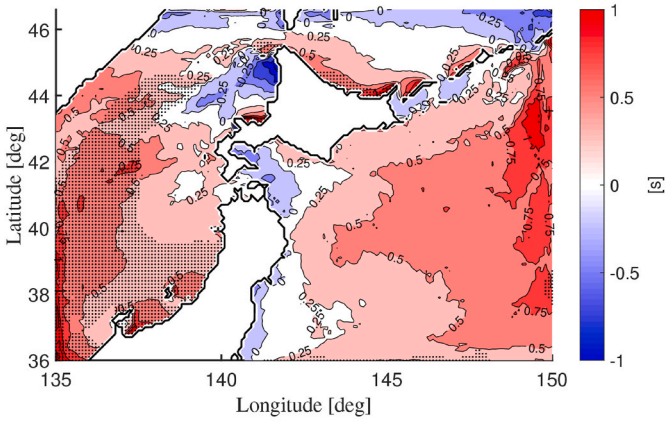

(b) Future change of ensemble average (contour line plots every 0.25 s, and black dotted area means that the future change is statistically significant.).

Fig. 14. Distribution of significant wave period when the maximum significant wave height occurs.

Declaration of competing interest

The authors declare that they have no known competing financial interests or personal relationships that could have appeared to influence the work reported in this paper.

Acknowledgements

We would like to thank Editage (www.editage.com) for English language editing.

References

Bärring, L., von Storch, H., 2004. Scandinavian storminess since about 1800. Geophys. Res. Lett. 31, L20202.
Booij, N., Ris, R.C., Holthuijsen, L.H., 1999. A third-generation wave model for coastal regions: 1. Model description and validation. J. Geophys. Res. 104 (C4), 7649–7666.
Bricker, J.D., Roeber, V., Fukutani, Y., Kure, S., 2015. Simulation of the December 2014 Nemuro storm surge and incident waves. J. Jpn. Soc. Civil Eng. 71, I_1543–I_1548.
Feser, F., Barcikowska, M., Krueger, O., Schenk, F., Weisse, R., Xia, L., 2015. Storminess over the north Atlantic and northwestern Europe—a review. Q. J. R. Meteorol. Soc. 141, 350–382.
Graham, N.E., Diaz, H.F., 2001. Evidence for intensification of north Pacific winter cyclones since 1948. Bull. Am. Meteorol. Soc. 82 (9), 1869–1894.
Gulev, S., Zolina, O., Grigoriev, S., 2001. Extratropical cyclone variability in the Northern Hemisphere winter from the NCEP/NCAR reanalysis data. Clim. Dynam. 17, 795–809.
IPCC, 2019. IPCC Special Report on the Ocean and Cryosphere in a Changing Climate.

Ishii, M., Mori, N., 2020. d4PDF: large-ensemble and high-resolution climate simulations for global warming risk assessment (review). Prog. Earth Planet. Sci. 7. https://doi.org/10.1186/s40645-020-00367-7. Article number 58.

Kawasaki, K., Mizutani, N., Iwata, K., Kobayashi, T., Yuhi, M., Saitoh, T., Kitano, T., Sumi, H., Mase, H., Yasuda, T., 2008. Field survey of damage due to February 2008 high wave on east coast of Toyama prefecture. Proc. Coast. Eng. 55, 151–155.

Kobayashi, Shinya, Ota, Yukinari, Harada, Yayoi, Ebita, Ayataka, Moriya, Masami, Onoda, Hirokatsu, Onogi, Kazutoshi, Kamahori, Hirotaka, Kobayashi, Chiaki, Endo, Hirokazu, Miyaoka, Kengo, Takahashi, Kiyotoshi, 2015. The JRA-55 reanalysis: general specifications and basic characteristics. J. Meteorol. Soc. Jpn. Ser. II 93 (1), 5–48. https://doi.org/10.2151/jmsj.2015-001.

Langenberg, H., Pzenmayer, A., von Storch, H., Sundermann, J., 1999. Storm-related sea level variations along the North Sea coast: natural variability and anthropogenic change. Continent. Shelf Res. 19, 821–842.

Lee, H.S., Kim, K.O., Yamashita, T., Komaguchi, T., Mishima, T., 2010. Abnormal storm waves in the winter East/Japan Sea: generation process and hindcasting using an atmosphere-wind wave modelling system. Nat. Hazards Earth Syst. Sci. 10, 773–792.

Mizuta, R., Yoshimura, H., Murakami, H., Matsueda, M., Endo, H., Ose, T., Kamiguchi, K., Hosaka, M., Sugi, M., Yukimoto, S., Kusunoki, S., Kitoh, A., 2012. Climate simulations using MRI-AGCM3.2 with 20-km grid. J. Meteor. Soc. Jpn. 90A, 233–258.

Mizuta, R., Murata, A., Ishii, M., Shiogama, H., Hibino, K., Mori, N., Arakawa, O., Imada, Y., Yoshida, K., Aoyagi, T., Kawase, H., Mori, M., Okada, Y., Shimura, T., Nagatomo, T., Ikeda, M., Endo, H., Nosaka, M., Arai, M., Takahashi, C., Tanaka, K., Takemi, T., Tachikawa, Y., Temur, K., Kamae, Y., Watanabe, M., Sasaki, H., Kitoh, A., Takayabu, I., Nakakita, E., Kimoto, M., 2017. Over 5,000 Years of ensemble future climate simulations by 60-km global and 20-km regional atmospheric models. Bull. Am. Meteorol. Soc. 98 (7), 1383–1398.

Mori, N., Shimura, T., Yoshida, K., Mizuta, R., Okada, Y., Temur, K., Ishi, M., Kimoto, M., Takayabu, Y., Nakakita, E., 2016. Mega-ensemble projection based on 60 km AGCM and its application to long-term impact assessment of storm surge. J. Jpn. Soc. Civil Eng. 72, 1471–1476 (in Japanese with English Abstract).

Mori, N., Chiwata, M., Ninomiya, J., Mase, H., 2017. Long-term variability of winter extratropical cyclones around Japan based on JRA-55 Analysis. J. Jpn. Soc. Civil Eng. 73, I_487–I_492 (in Japanese with English Abstract).

Murata, A., Sasaki, H., Hanafusa, M., Kurihara, K., 2013. Estimation of urban heat island intensity using biases in surface air temperature simulated by a nonhydrostatic regional climate model. Theor. Appl. Climatol. 112, 351–361.

Ranasinghe, R.S., Fukase, Y., Sato, S., Tajima, Y., 2010. Locally concentrated damage at Shimoniikawa Coast, Toyama Bay, Japan due to giant swell waves. Proc. Coast. Eng. 1, 25.

Sanders, F., Davis, C.A., 1988. Patterns of thickness anomaly for explosive cyclogenesis over the west-central north Atlantic ocean. Mon. Wea. Rev. 116, 2725–2730.

Saruwatari, A., de Lima, A.C., Kato, M., Nikawa, O., Watanabe, Y., 2015. Report on the 2014 winter cyclone storm surge in Nemuro, Japan. Coast. Eng. J. 57, 1550014.

Sasaki, H., Murata, A., Hanafusa, M., Oh'izumi, M., Kurihara, K., 2011. Reproducibility of present climate in a non-hydrostatic regional climate model nested within an atmosphere General Circulation Model. SOLA 7, 173–176.

Shimura, T., Mori, N., Yasuda, T., Mase, H., 2014. Projection of future ocean wave extremes based on MRI-AGCM3.2H ensemble experiments. J. Jpn. Soc. Civil Eng. 70, 1266–1270 (in Japanese with English Abstract).

Tamura, H., Kawaguchi, K., Fujiki, T., 2020. Phase-Coherent amplification of ocean swells over submarine canyons. J. Geophys. Res.: Oceans 125, e2019JC015301.

Yoshida, A., Asuma, Y., 2004. Structures and environment of explosively developing extratropical cyclones in the Northwestern Pacific region. Mon. Weather Rev. 132, 1121–1142.